

Zeolite-inspired 3d printed structures with enhanced mechanical properties

Rushikesh S. Ambekar^{1†}, Eliezer F. Oliveira^{2,3,4†}, Brijesh Kushwaha¹, Leonardo D. Machado⁵, Mohammad Sajadi², Ray H. Baughman⁶, Pulickel M. Ajayan², Ajit K. Roy⁷, Douglas S. Galvao^{3,4*}, Chandra S. Tiwary^{1,2*}

¹Metallurgical and Materials Engineering, Indian Institute of Technology Kharagpur, Kharagpur-382355, India

²Department of Material Science and NanoEngineering, Rice University, Houston, Texas, 77005 United States

³Applied Physics Department, State University of Campinas (UNICAMP), Campinas, SP, Brazil

⁴Center for Computational Engineering & Sciences (CCES), State University of Campinas - UNICAMP, Campinas, SP, Brazil

⁵Department of Theoretical and Experimental Physics, Federal University of Rio Grande do Norte (UFRN), Natal, RN, Brazil

⁶Alan G. MacDiarmid NanoTech Institute, The University of Texas at Dallas, Dallas, Texas, 75080-3021, United States

⁷Materials and Manufacturing Directorate, Air Force Research Laboratory, Wright Patterson AFB, OH 45433-7718, United States

† Equal contribution

Email: chandra.tiwary@metal.iitkgp.ac.in (C.S.T) and galvao@ifi.unicamp.br (DSG)

Abstract

Specific strength (strength/density) is a crucial factor while designing high load bearing architecture in areas of aerospace and defence. Strength of the material can be enhanced by blending with high strength component or, by compositing with high strength fillers but both the options has limitations such as at certain load, materials fail due to poor filler and matrix interactions. Therefore, researchers are interested in enhancing strength of materials by playing with topology/geometry and therefore nature is best option to mimic for structures whereas, complexity limits nature mimicked structures. In this paper, we have explored Zeolite-inspired structures for load bearing capacity. Zeolite-inspired structure were obtained from molecular dynamics simulation and then fabricated via Fused deposition Modeling. The atomic scale complex topology from simulation is experimentally synthesized using 3D printing. Compressibility of as-fabricated structures was tested in different direction and compared with simulation results. Such complex architecture can be used for ultralight aerospace and automotive parts.

1. Introduction

The researchers have developed copious materials for load-bearing applications which include metals, ceramics and polymers, out of which polymers are most preferred material due to its low density, high specific strength, tailor-ability; on the other hand, metals have higher density and ceramics are brittle and have poor processability^[1-3]. Furthermore, load-bearing capability of pristine polymer enhanced by blending or with interpenetrating network in which compatibility between polymers can limit the selection of polymers^[4]. Recently, composites attracted researchers due to compensation of one materials limitation by another material-Composite consist of matrix (polymer resin) and reinforcement (mostly ceramic or metal) where matrix helps in ease of processing and reinforcement bear the load, but at critical load slippage of reinforcement from the matrix is experience due to poor matrix-reinforcement interaction as matrix and reinforcement are different class of materials^[5]. Therefore researchers have shifted towards the design-oriented approach instead of morphological strengthening approach^[6].

The geometry of the pore and pore size are essential part of design as these are one of the key factors which decide the mechanical strength of the structure. Pore shapes such as cubic, spherical, cylindrical, octahedral, tetrahedral contribute structural advantage under load^[7]. Nature already have highly porous yet complex structure which inspired researchers for biomimetic design like aeroplane inspired by birds^[8], design of Gherkin tower situated in London inspired by the venus flower basket^[9], self-cleaning surfaces inspired by gecko feet^[10], hydrophobic surfaces inspired by silver ragwort leaf and lotus leaf^[11], artificial bone inspired by natural bone^[12] and synthetic shark skin inspired by shark texture to reduce drag^[13]. In spite of numerous successful biomimicry of nature, it is difficult due to extreme complexity, limitation of materials properties.

Therefore researchers are interested in the easy processable but complex structure for enhanced load-bearing function^[14].

There are copious techniques available to fabricate porous structures such as gas foaming^[15], solvent casting/particulate leaching^[16] and 3D printing, out of which 3D printing is most desired candidate for porous structure due to its ability to fabricate intricate structure, cost-effectiveness, scalability, controlled porosity (size and shape)^[17]. Kaur *et al.* fabricated cellular truss inspired structure via 3D printing technique. Three different materials such as nylon, poly(lactic acid) (PLA), and Carbon fiber reinforced PLA (CFRPLA) were fabricated with octet and octahedral pore geometry. The compression test shows that of CFRPLA octet structure (0.37 GPa) has higher young's modulus than PLA octet structure (0.29 GPa) similarly, CFRPLA octahedral structure (0.58 GPa) has higher young's modulus than PLA octahedral structure (0.45 GPa)^[18]. Belhabib *et al.* developed mathematical model inspired Acrylonitrile Butadiene Styrene porous cellular structure. The compression study reveals that varying pore density in the cellular structure, compression strength varies from 2.7 to 6.3 MPa^[19]. Naghieh *et al.* reported poly (lactic acid)/gelatin-forsterite scaffolds via combination of 3D printing and electrospinning technique. Effect of extruder temperature on mechanical properties have been studied such as pristine PLA structure printed at 210°C (0.12 GPa) has higher elastic modulus than printed at 192°C (0.11 GPa) temperature^[20].

Recent studies have shown that combining computational modeling with 3D printing technology is an effective way to generate new structures using geometric design principles^[21,22]. This approach opens new and quite interesting perspectives to design new materials with enhanced mechanical properties. One recent example of this is the structural and mechanical properties of 3D printed macroscale (cm size) schwarzite crystals generated from fully atomistic models^[21].

Schwarzites are 3D porous carbon-based structures idealized by Mackay and Terrones^[23] that exhibit positive and negative curvature topologies with tunable porous size and shape, and fascinating properties^[24–29]. This study showed that the qualitative tendencies observed in the mechanical properties of schwarzites structures (carbon-based) from Molecular Dynamics simulations, such as deformation patterns, high failure strain, and Young's modulus values, agree very well with the observed from the experimental 3D printed schwarzite structures (printed using PLA). In this way, to generate corresponding macroscale structures of atomic-scale structural models has proven to be an effective approach to build new structures with structural and mechanical improvements.

Carbon based nanostructures with complex geometries have been intensively studied. Depending on the architectural geometry of these structures, remarkable mechanical and electrical properties are obtained^[30–34]. As the study of Schwarzites has shown that carbon-based nanostructures with complex geometries can be used as templates for 3D printed macroscale structures and its properties follow similar patterns observed at the nanoscale^[21], it will be interesting to look for other nanostructures to be used as 3D printing template.

Recent studies have point out that a feasible approach to produce new carbon-based nanostructures with interesting geometries is to use zeolites as templates^[35–37]. Zeolites are, in general, aluminosilicates whose structures are composed of several pores and channels of molecular sizes, which allow building 3D porous nanostructures inside them. Thus, it will be interesting to study the properties of these possible formed structures inside the zeolites pores and select those that present desired mechanical properties to be 3D printed at macroscale.

In this work, 3D printing technique, in particular fused deposition modeling, was utilized to fabricate zeolite-based structure for load-bearing function. The compression strength of PLA

porous structure was investigated experimentally and theoretically and effect of varying pore density on compression strength was also studied. In addition, the effect of layer deposition orientation on compression property was also investigated.

2. Materials and Method

2.1 Obtaining the beta zeolite-based models

Here we will give a short description on how the studied structures were obtained; the complete description can be found in the previous work of Oliveira et al.[38]. Our structure models were based in the beta zeolite (BEA framework type, composed by Si and O atoms, P4₁22space group, and unit cell parameters $a=b=12.63 \text{ \AA}$, $c=26.18 \text{ \AA}$, $\alpha=\beta=\gamma=90^\circ$ with 3840 atoms_[39]. The BEA has two orthogonal and equivalent channels that partially intersect (along the y and z directions). To form nets inside the BEA channels, first we had to look for the single wall carbon nanotubes (CNT) candidates that fit inside the BEA channels. To do so, we tested CNT with different chiral indices (n,m) inside the BEA channels and we performed the geometry optimization of the systems BEA+CNT in order to determine which CNT keep the system energy the lowest. These calculations were performed with Molecular Mechanics (MM) simulations using the well-known Universal Force Field (UFF)_[40], as implemented in the Forcite software_[41]; an energy convergence tolerance of 0.001 kcal/mol and a force convergence tolerance of 0.5 kcal/mol/ \AA were adopted. The size and shape of the unit cell was also optimized. In this step we used a large BEA periodic supercell with 12.3 nm along its channels, and the CNT length was fixed in 10 nm (their number of atoms depends on the CNT chirality), and the tube length was kept fixed in 10 nm. The large BEA supercell was used to prevent spurious inter-nanotube interactions. The CNTs with chiralities (3,3), (4,2), (5,1), (6,0), (4,3), and (5,2) resulted in the most

stables BEA+CNT structures (similar energies). As the minimum energy of all was observed when the CNT (6,0) was inserted into the BEA channels, we used it to design our carbon networks.

To build the network structures, we had to create (energetically favorable) junctions between the chosen CNT. Then two CNT (6,0) were inserted into the adjacent BEA channels (along the y and z directions, see Structure 1 in Figure 1). We fixed the CNTs positions and they were removed from the BEA. We removed the carbon atoms in the region in which the CNTs were close to each other and non-bonded carbon atoms were added into the space between the CNTs. Using Molecular dynamics (MD) simulations with the ReaxFF force field^[42], as implemented in the computational package LAMMPS^[43], we let this system evolve until a junction between the CNTs was created. In this step, the positions of the CNTs was kept fixed and various cycles of heating and cooling with a temperature range from 300 K to 1500 K were performed to produce a defect-less junction between the CNTs. These calculations were controlled using the Nosé-Hoover thermostats, and a timestep of 0.2 fs. After these steps, a “X” type junction was obtained between the CNTs, which is formed from jointed heptagons and pentagons^[44]. Then, the jointed CNTs were inserted again into the BEA in order to verify if the created junction fit inside the empty space initially present between CNTs and create unit cells that could be replicated into a periodic 3D structure.

Deciding the CNT and the junctions that would be employed to build the network structures, we considered two different cases: one with partial filling of BEA channels (Structure 1 in Figure 1) and one with total filling of BEA channels (Structure 2 in Figure 1). These structures presented in Figure 1 were built from their corresponding unit cell reproduction. The unit cell parameters of these two carbon network are: 894 carbon atoms, mass density of 0.44 g/cm³, a=28.47 Å, b=39.93 Å, c=39.22 Å, and $\alpha=\beta=\gamma=90^\circ$ for Structure 1 and 321 carbon atoms, mass

density of 1.28 g/cm³, a=12.99 Å, b=13.68 Å, c=29.28 Å, and $\alpha=\beta=\gamma=90^\circ$ for Structure 2. A thermal equilibration for temperatures of 300 K to 600 K was done for both structures in order to verify its thermal stability; the structures remain stable.

2.2 Preparation of the structures for 3D printing

After obtaining the structures from MM/MD studies, we created the structures to be printed and the mechanical properties evaluation. Using VMD software^[45], we create the Structures 1 and 2 supercells of approximately the same volume of 20.104Å³; these structures are presented in Figure 1. In order to compare the behavior of the BEA with the structures created from its channels filling, we replace its original atoms (Si and O) by carbon atoms. Using a similar procedure described before, we tested the stability of this carbon-based BEA and the Structure 3 supercell (see Figure 1) was created with approximately the same size of the Structure 1 and 2. The data of these carbon-based structures are presented in Table 1. Then, these structures were exported to a stereolithography file (STL) to be printed.

Then, the structures were designed in Molecular Dynamics and fed in the FDM printer as a G-Code program; front view and 3D view of the molecular structure are shown in **Figure 1 (a)** and **Figure 1 (c)** respectively. Designed structures are successfully fabricated in Flashforge adventure 3 printer, the front view and 3D view of printed structures are illustrated in **Figure 1 (b)** and **Figure (d)** respectively. The precise dimensions of these fabricated structures are depicted in **Table 1**.

The commercial-grade of solid Polylactic acid (PLA) filament was fed into the printer which is then subsequently heated in extruder at 210°C and extruded through nozzle on the heated bed at 50°C during printing. The paper tape was utilized for better adhesion of structure to the

printer bed, as fabricated structures have single-layer thickness of 180 μm in the z-direction along with 100% fill density. PLA filament (white) was provided by Flashforge 3D Technology Co. Ltd. (Zhejiang, China) and has a diameter of 1.75 mm (with tolerance ± 0.1), mass density of 1.210-1.430 gm/cm^3 and melting point 190°C to 220°C.

2.3 Compressive mechanical tests

Due to the structures be equal along the y and z directions (see Figure 1), the load-bearing capacity of the post-fabricated structures was tested in x and z directions using the UTM SHIMADZU (AG 5000G), with a compression displacement rate maintained at 1 mm/min.

For a qualitative comparison, we also performed the compressive tests in the molecular Structures 1, 2 and 3 using MD simulations. To do so, the finite structures were placed atop a fixed 12-6 Lennard-Jones wall ($\epsilon = 0.07$ kcal/mol and $\sigma = 3.55$ Å) and above of them, a movable 12-6 Lennard-Jones wall ($\epsilon = 0.07$ kcal/mol and $\sigma = 3.55$ Å) was placed. With the movable wall, a compressive uniaxial strain was applied to deform the structure and evaluate its mechanical response with a strain rate of -10^{-6}fs^{-1} . In order to decrease the thermal contribution in our deformation tests, these simulations were done at 10 K in an NVT ensemble. The stress-strain curve was built using the virial stress tensor component and the engineering strain at each compressive direction. In order to determine the spatially concentrated stress during simulations, we evaluated it through the von Mises stress, the second invariant of the deviatoric stress tensor^[46]. This analysis also provides us insights about the fracture dynamics. All deformation tests were performed using the ReaxFF force field^[42], with a timestep of 0.1fs.

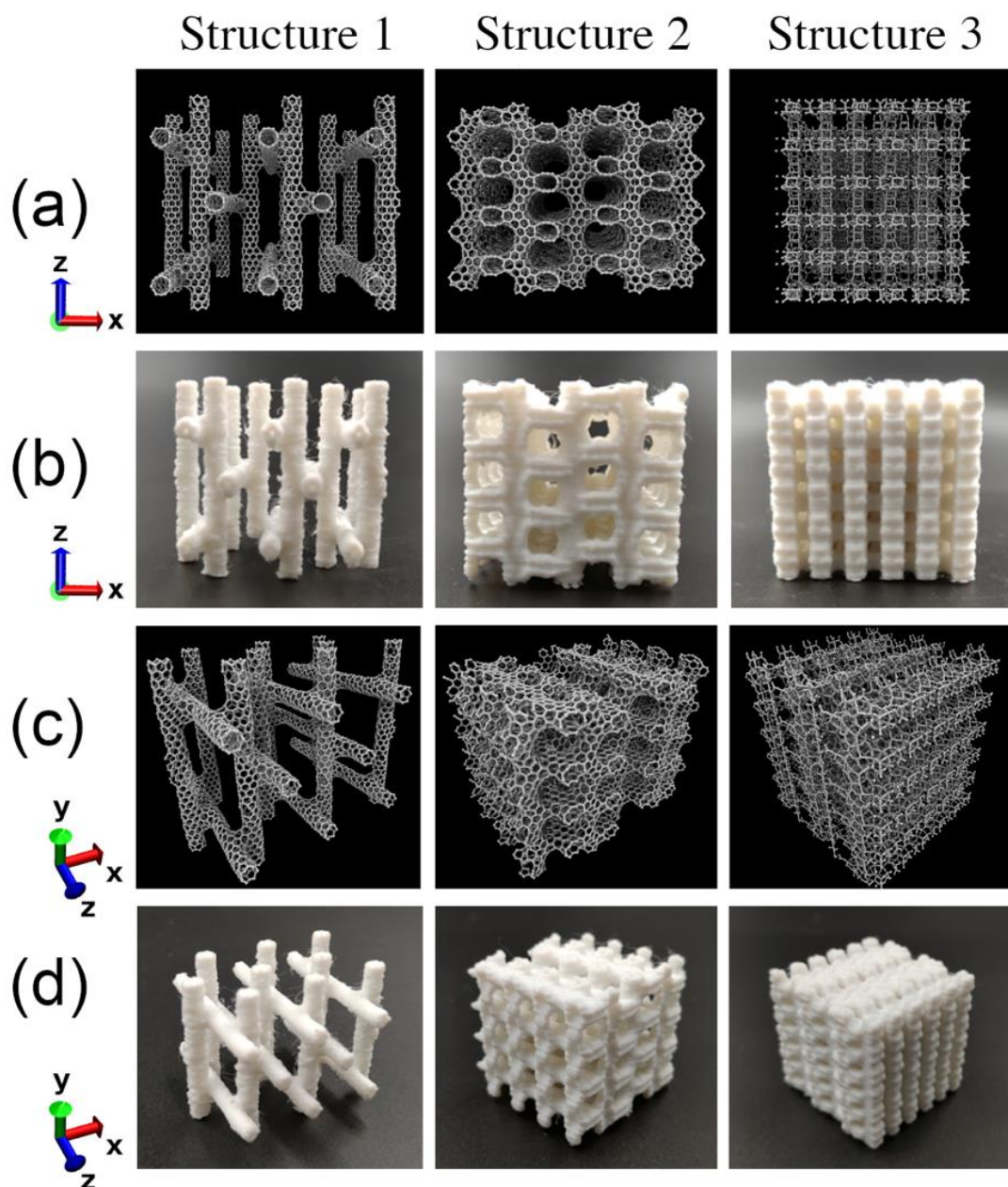


Figure 1. a) Front view of zeolite-inspired molecular structures. b) Front view of 3D printed zeolite-inspired structures. c) 3D view of zeolite-inspired molecular structures. d) 3D view of 3D printed zeolite-inspired structures.

Table 1. Specifications of the created molecular structures from MD simulation and the 3D printed corresponding ones.

Sample Name	Theoretical MD		3D Printed	
	Number of carbon atoms	Dimensions (Å)	Dimensions (cm)	Weight (gm)
Structure-1	16,944	78 x 75 x 71	3.0 x 2.955 x 3.044	17.560
Structure-2	10,799	62 x 50 x 56	3.0 x 2.994 x 2.869	11.5565
Structure-3	6,310	78 x 62 x 59	3.0 x 2.615 x 2.646	3.002

3. Results and Discussion

In order to have an initial idea of the mechanical behavior of the Structures 1, 2 and 3, we will present the theoretical findings from MD simulation. In Figure 3 is shown the theoretical stress-strain curves for compressive tests conducted in x (Figure 3(a)) and z-direction (Figure 3(b)) for Structures 1, 2, and 3. Table 2 presents some mechanical properties data found in Figure 3. The Structures 1, 2, and 3 have porosities of, respectively, 47.52%, 63.83%, and 88.42%. As can be seen, the curves representing the compressive tests in both x and z-directions presents a similar behavior regarding the stress values, in which the higher stresses are observed for less porous structure, followed by the intermediary and the higher porous structures. This indicates that the porosity of the structures influences the stress level supported by them. In Figure 3(a), in which it is related to the compressive test in x-direction, indicate a relatively short elastic region for the structures 2 and 3, in which a yield strength and stress of 3.7GPa and 1.2 % and 4.8 GPa and 0.8 % is observed, respectively. As for structure 1, the most porous one, a very long elastic regime is seen when compressed along x-direction, with a yield strength of 0.6 GPa for a strain around 60%.

These results suggest that the porosity play a crucial role regarding the deformation of the structure: the less porous structure, the shorter is its elastic regime and more stress is necessary to cause some deformation and achieve the plastic regime of the structure.

In Figure 3(b) it is shown the theoretical stress-strain curve for compressive tests conducted in z-direction. As can be noticed, the shape of the stress-strain curves of compressive test in z-direction of structures 2 and 3 resemble with the same found in x-direction; despite this similarity, the yield strength and strain are different. We found a yield strength and strain for compressive test in z-direction of 3.6 GPa and 4.2 % and 3.9 GPa and 1.1 %, respectively, for structures 2 and 3. These values are lower that the same found for compressive test in x-direction. As for structure 1, a different behavior is seen in Figure 3(b) in comparison with Figure 3(a). Structure 1 do not present a high elastic behavior in z direction, in which yield strength of 1.8 GPa at around 2.4 % of strain is found. These results indicate that beyond the porosity of the structure, the orientation also influence the observed mechanical properties. In general, we can see that the direction that is perpendicular to the nanotubes disposition, that is x-direction, presents the toughest and elastic structures with decreasing the porosity.

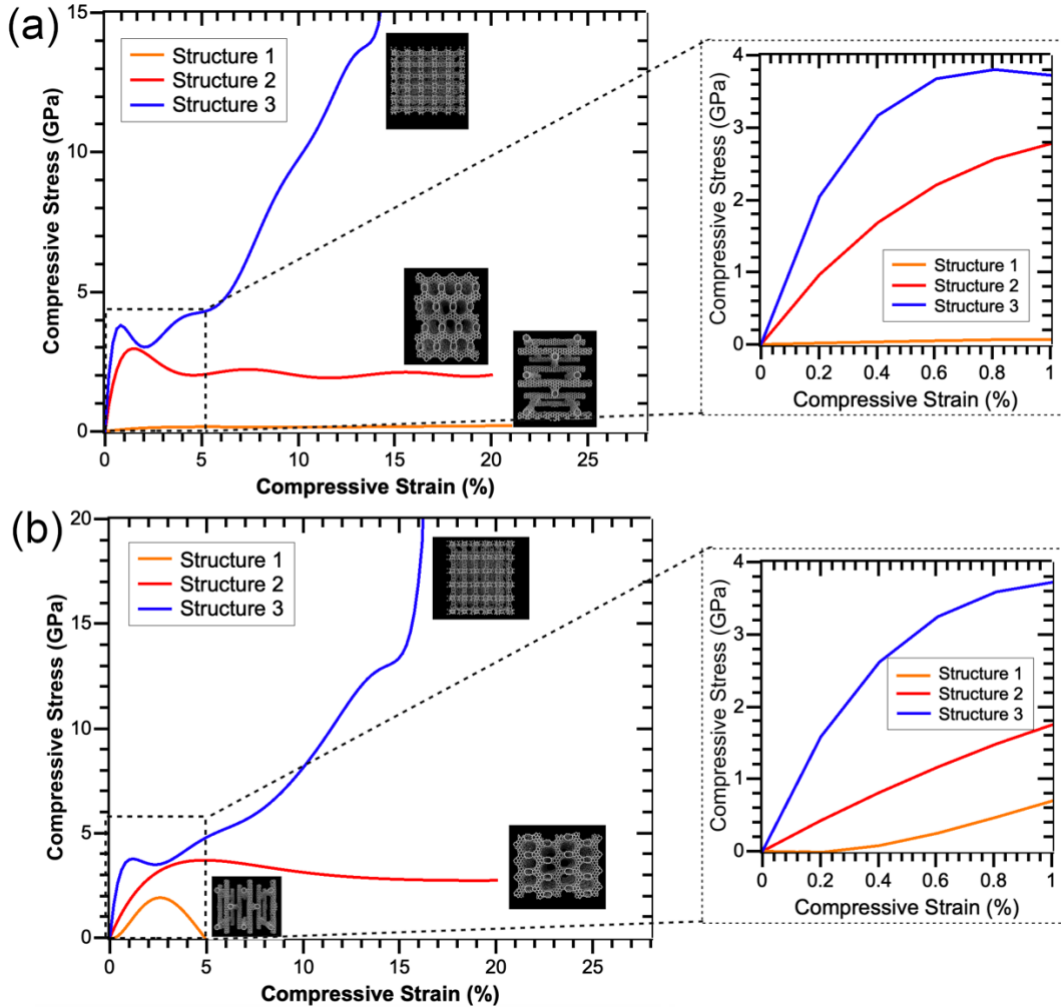


Figure 2. Theoretical stress-strain curves from MD simulations for compressive tests in (a) x-direction and in (b) z-direction of structures 1, 2, and 3.

The stress-strain curve of PLA printed structures is depicted in Figure 4. Comparing these experimental data with the same found in the theoretical data presented in Figure 3, a good qualitative behavior is found for the stress-strain curves. This is an indication that the mechanical behavior found in molecular system can be qualitatively observed in 3D printed structures that follows the same geometrical construction, as also seen before [21]. In this way, mimicking the molecular structures shows to be an important tool to engineer new macro-structures for load-bearing applications.

In Figure 4(a) shows that experimental stress-strain curve for compressive test of structures 1, 2, and 3 in x-direction. Following the observations of MD simulations, the crucial role of the porosity in mechanical strength is also clear, since compression curves confirms that high-density structure (such as structure 3) can withstand at high compressive load, whereas low-density structure (such as structure 1) can carry low compression load. In the present research, we have fabricated structures in fused deposition modelling type 3D printer, therefore, polymeric chains are oriented in x and y direction which are responsible for anisotropic nature of as-prepared structures. The printed structures are susceptible to early failure when compressive load applied in x-direction compare to compressive load applied in the z-direction.

As represented in Figure 4(b) for z-direction, the compressive load is applied in transversely on polymeric chains, therefore, the structure can accommodate higher load before deformation. The applied compression stress densifies the structure over the period of deformation, therefore, strength of structure accelerated once all the pores are deformed. For further study, young's modulus, yield strength and toughness of as-printed structures were extracted from compressive stress vs compressive strain curve (as depicted in **Table 2**).

The porosity of structure on young's modulus and yield strength are clear in both x and z-direction. The structure-1 has highest porosity of 88.4% and therefore it has lower compression strength than structure 2 and structure 3. Young's modulus of structure 1 in z direction (89.3 MPa) was greater than structure-1 in x-direction (9.8 MPa). In x-direction, structure 3 (202.36 MPa) has higher young's modulus than structure 2 (162.88 MPa); similarly, in z-direction structure 3 (190.39 MPa) has higher young's modulus than structure 2 (92.159 MPa) owing to structure 2 (63.83%) has higher porosity than structure 3 (47.52%). Yield strength of structure 2, structure 3 in x direction and structure 2, structure 3 in z-direction are 7.60, 11.20, 3.82, 9.52 MPa respectively. It

was observed that orientation of structures has huge effect on toughness, i.e., porous structure tested in x-direction have 50% reduced toughness compared to Z-direction. As it can be noticed in Table 3, the qualitative comparison between the experimental and theoretical data for mechanical properties indicates a quite good according. Lastly, the toughness of structure 2 (380KJ/m³) and structure 3 (1045 KJ/m³) in z-direction are higher than structure 2 (200 KJ/m³) and structure 3 (540 J/m³) in x-direction.

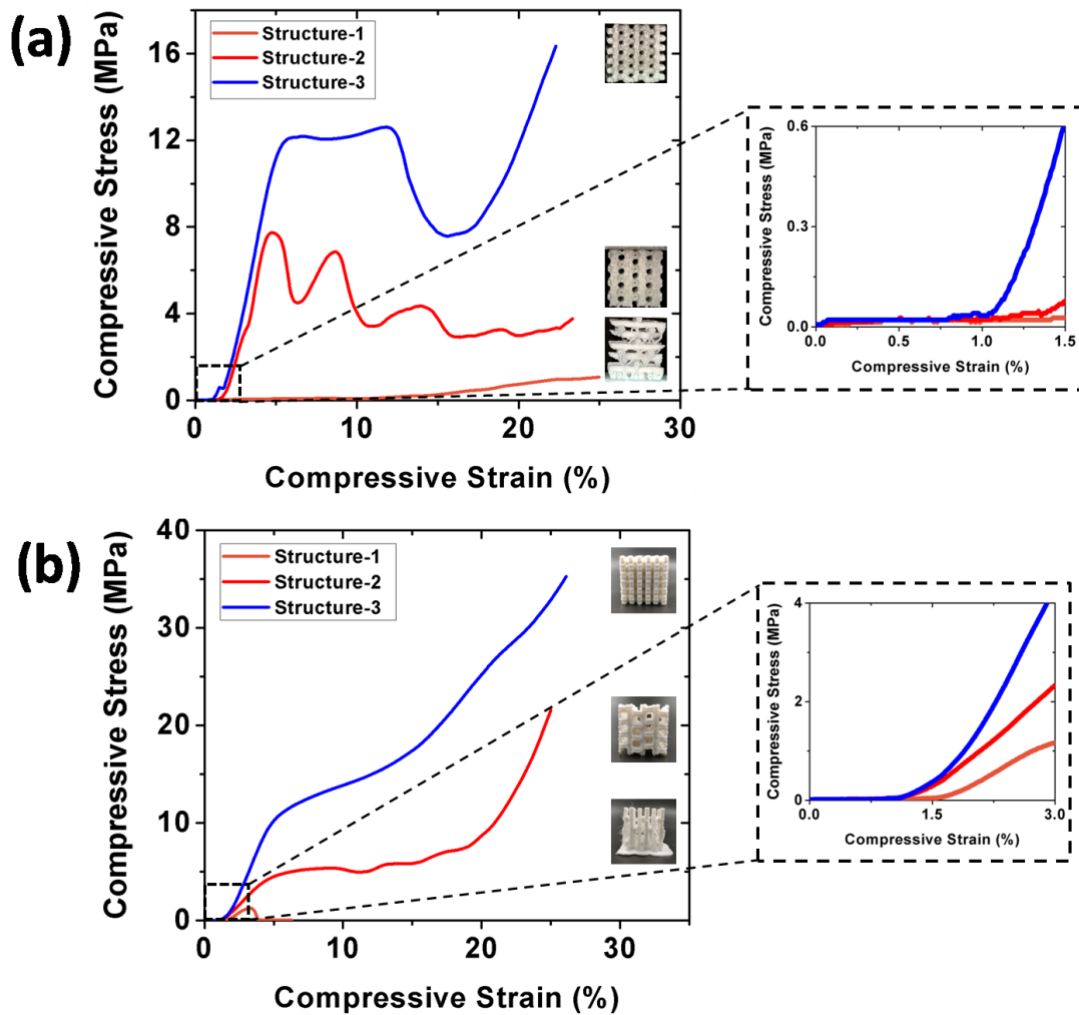


Figure 3. Experimental stress-strain curves for compressive tests in (a) x-direction and in (b) z-direction of structures 1, 2, and 3.

Table 3. Mechanical properties data derived from experimental and theoretical compressive tests.

The theoretical data from MD simulations are presented into parentheses.

Orientation	x-direction			z-direction		
	1	2	3	1	2	3
Porosity (%)	88.4	63.8	47.2	88.4	63.8	47.2
Young's Modulus	9.8 MPa (6.9 GPa)	162.9MPa (214.1GPa)	202.4MPa (261.8 GPa)	89.3 MPa (80.0 GPa)	92.2 MPa (160.1 GPa)	190.4 MPa (277.6 GPa)
Yield Strength	0.99 MPa (0.6 GPa)	7.6 MPa (3.7 GPa)	11.2MPa (4.8 GPa)	1.24 MPa (1.8 GPa)	3.8 MPa (3.6 GPa)	9.5MPa (3.9 GPa)
Yield Strain	23.78 % (60.0 %)	4.5% (1.2%)	5.0% (0.8%)	3.27 % (2.4 %)	4.1% (4.2 %)	4.6% (1.1 %)
Toughness (KJ/m ³)	73.1	200	540	12	380	1045

In order to understand the load-bearing behavior of structures at a microscopic level, we have captured snapshots of porous structures at some selected compression strain percentage during compression test. These data are shown in Figures 4 and 5, along with the corresponding one from the MD simulations. The theoretical MD snapshots are colored according to the distribution of the Von Mises stress along the compressive tests; the local stress level is indicated on stress level bar.

The structures tested in x-direction clearly shows that non-uniform compression of pores as the crack can be easily initiated between two printed layers which cause poor load distribution (as shown in **Figure 4**).The theoretical data indicates that the stress is most concentrated at the nanotube junctions, and the failure of the structure is reach with the collapse of the pores and nanotubes. As can be seen, the high elasticity of the structure 1 in x-direction can be related to the easily slipping nanotubes. As this structure have a very high porosity and low junctions between

the nanotubes, these ones can easily slip and be accommodated at the existing empty spaces without a collapse.

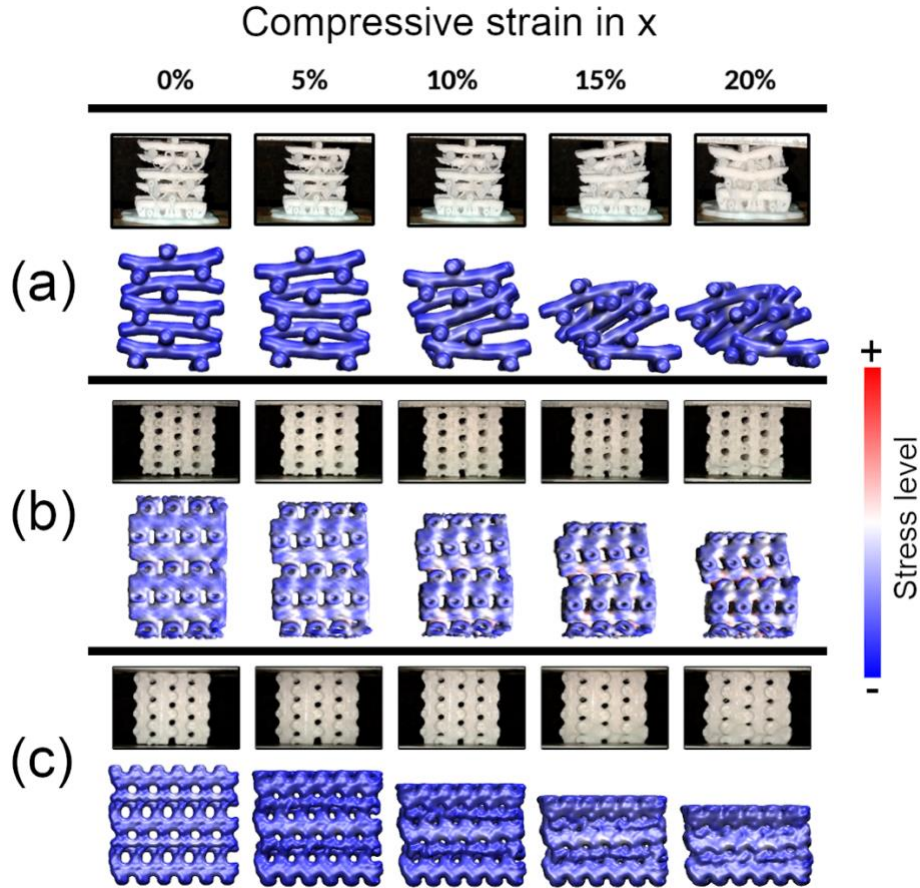


Figure 4. Snapshots of experimental and theoretical compressive tests in x-direction of structures (a) 1, (b) 2, and (c) 3. For the theoretical ones, it is presented the distribution of the Von Mises stress (according to the color bar of stress level) along the compressive test.

The structures tested in z-direction have a uniform compression due to compression load applied in transverse direction (as shown in **Figure 5**). Differently from the observed for x-direction, the most stressed part of the structures are the nanotubes, that are disposed parallel to the

compressive direction. The failure of the structures in z-direction are most related to the nanotubes bending.

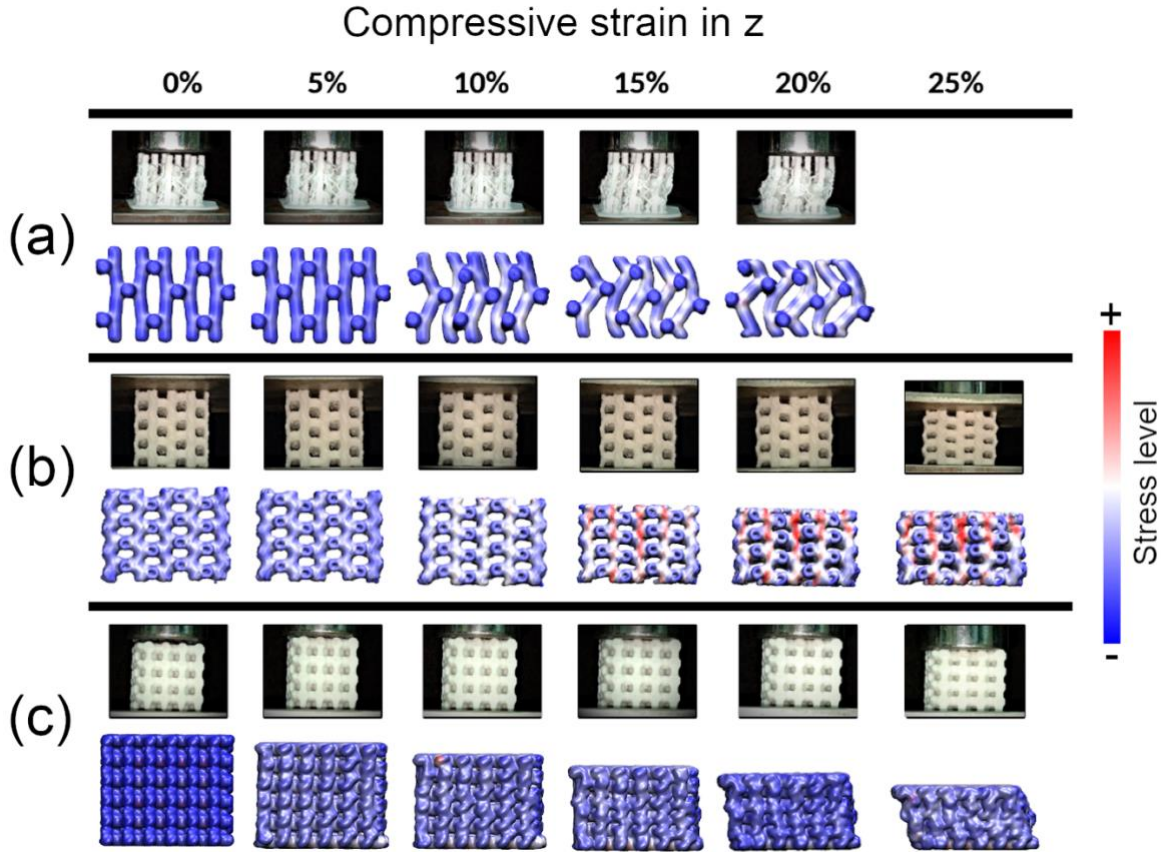


Figure 5. Snapshots of experimental and theoretical compressive tests in z-direction of structures (a) 1, (b) 2, and (c) 3. For the theoretical ones, it is presented the distribution of the Von Mises stress (according to the color bar of stress level) along the compressive test.

To have an idea on how the deformations and failure of these happens, it is interesting to take a look into the characteristic and behavior of the resulting templated structures from Beta zeolite. As seen before, the molecular structures that can be created from the Beta zeolite (circular) pores results in a net of jointed carbon nanotubes. When these structures are printed into macroscale, the resulting structures can be regarded as a jointed cylindrical structure, as depicted

in Figure 6(a). When the templated structures are submitted to compressive stress, if they were not jointed, the cylinders/nanotubes could be free to go to a rolling and slipping process in order to accommodate the stress (see Figure 6(a)). As the cylinders/nanotubes are jointed, we add a resistance to rolling and slipping, which results in a stress accumulation in the jointed regions.

Clearly the number of joints also determines the degree of freedom of cylinders/nanotubes. The smaller the number of joints, the more stress will be distributed along the structure due to the cylinders/nanotubes rolling and slipping. As can be seen in Figures 6(b) and 6(c), in which a representative part of the structures is shown, compression perpendicular to cylinders/nanotubes (x-direction) tends to make them rotate and bend to accommodate stress. In the case of high-density structure (structure 2), the number of joints is higher which decrease the rolling/slipping freedom of the cylinders/nanotubes; this results a smaller range of motion in the perpendicular directions to the compressive one. Then, the stress becomes more concentrated at the junctions and the stress yield is reached when the nanotubes can no longer roll and slip, which leads to the collapse of the cylinder/nanotube (see Figure 6(c)). As for the low-density structure (Structure 1), the number of joints is smaller, which makes the structure freer to accommodate new conformations as we increase the stress. Because of this, when this structure is compressed in the x-direction, the rolling and slipping process allow it to spread as we compress it (see Figure 4(a)), so that it is not seen the nanotube collapse, but a bending when the cylinders/nanotubes rolls (Figure 6(b)).

When the compression is parallel to cylinders/nanotubes (z-direction), we see that cylinders/nanotubes have difficulty to roll and slip, which leads to a stress accumulation at parallel portions to the compressive one, i.e., the cylinders/nanotubes. Initially, the joints concentrate more stress than the cylinders/nanotubes, since they are trying to roll (start a pull-push process at the junctions in a tentative to roll). Then, as seen in Figures 6(b) and 6(c), the stress tends to dissipate

perpendicular to junctions. Because junctions withstand high stress without breaking, so does not the nanotube, so we can see that they begin to bend, which leads to the structure to collapse. Then, in compression perpendicular to the cylinders/nanotube, the failure of the structures is more related to the bending yield.

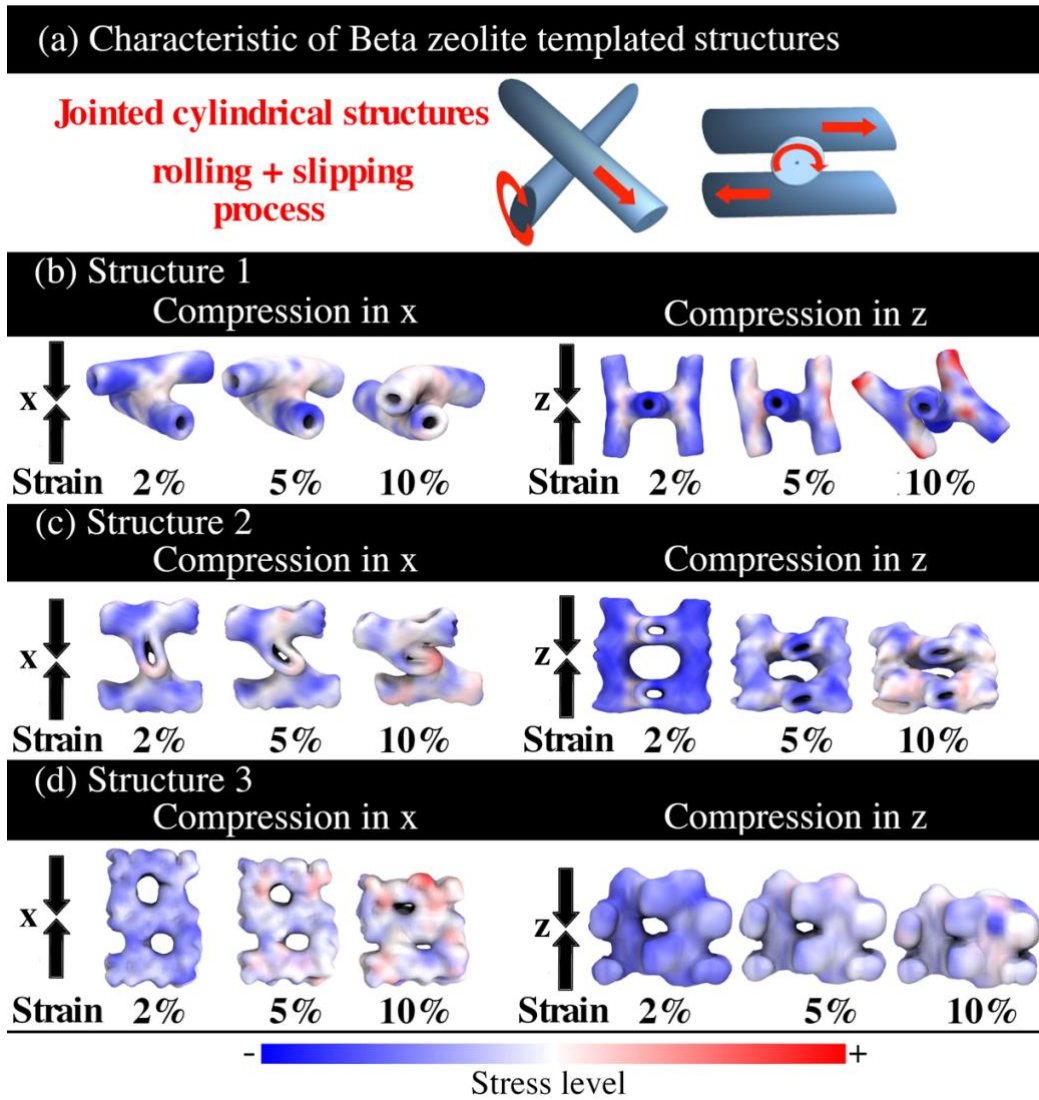


Figure 6. (a) Characteristics of beta zeolite template structure and compression snapshots at junctions of the structure-1, (c) structure-2 and (d) structure-3 in x and z-directions.

For the Beta zeolite structure (structure 3), taking a look at it in Figure 1, we can see that it resembles an interpenetrated quasi-parallelepiped net with quasi-circular porous. Compared to structures 1 and 2, we can say that the Structure 3 have a very high number of junctions and more matter. When structure 3 is compressed in x- or z-direction, we saw that the stress is more delocalized along the structure (Figures 4(c) and 5(c)). Looking at a small portion, as in Figure 6(d), it is possible to see that the failure of the structure occurs when the quasi-paralepidid structure fails around the zeolite channel, leading this one to a collapse. This happens due to the scarce freedom of the quasi-paralepidid building block, that are unable to roll and slip easily; this also draws attention to the geometric question, since circular cross section shape has a greater ease of accommodation and movement than those of square cross section. In general, we can conclude that the resistance of the studied structures can be related to the amount of the junctions to form a net, as well as the geometrical 3D shape of the net constituents.

4. Conclusions

In this work, we have explored effect of geometry on compressibility of zeolite-inspired 3D printed structures, Elongation of Structure 1 in X direction shows poor strength therefore it has 23.78% yield strain experimentally and 60% in theoretically due to anisotropic nature of 3D printed structure. Theoretically, structure-3 in z-direction (277.6 GPa) has higher Young's modulus than structure-3 in x-direction (261.8 GPa) but experimentally, structure-3 in z-direction (190.4 MPa) has higher Young's modulus than structure-3 in x-direction (202.4 MPa). It is also observed that energy absorption capacity of structure 3 in z-direction (1045 KJ/m³) enhanced by 2-fold compared to structure 3 in x-direction (540 KJ/m³).

5. Acknowledgement

EFO and DSG thank the Brazilian agencies CNPq and FAPESP (Grants 2013/08293-7, 2016/18499-0, and 2019/07157-9) for financial support. Computational support from the Center for Computational Engineering and Sciences at Unicamp through the FAPESP/CEPID, the Center for Scientific Computing (NCC/GridUNESP) of São Paulo State University (UNESP), and the High-Performance Computing Center at UFRN (NPAD/UFRN) are also acknowledged. This study was financed in part by the Coordenação de Aperfeiçoamento de Pessoal de Nível Superior - Brasil (CAPES) –Finance Code 001.

6. References

- [1] S. R. Allen, *J. Mater. Sci.* **1987**, *22*, 853.
- [2] S. Cheng, J. A. Spencer, W. W. Milligan, *Acta Mater.* **2003**, *51*, 4505.
- [3] J. Yang, W. Liu, L. Zhang, B. Xiao, *Constr. Build. Mater.* **2009**, *23*, 687.
- [4] P. Sakellariou, *Polymer (Guildf)*. **1993**, *34*, 3408.
- [5] L. Yang, Y. Yan, Y. Liu, Z. Ran, *Compos. Sci. Technol.* **2012**, *72*, 1818.
- [6] P. Zhang, J. Liu, A. C. To, *Scr. Mater.* **2017**, *135*, 148.
- [7] S. Wang, Z. Zheng, C. Zhu, Y. Ding, J. Yu, *Mech. Mater.* **2018**, *127*, 65.
- [8] E. Lurie-Luke, *Biotechnol. Adv.* **2014**, *32*, 1494.
- [9] Robin Koontz, in *Biomimic Build.*, Carson-Dellosa Publishing, **2018**, pp. 28–35.
- [10] S. Sethi, L. Ge, L. Ci, P. M. Ajayan, A. Dhinojwala, *Nano Lett.* **2008**, *8*, 822.

- [11] J. Lin, Y. Cai, X. Wang, B. Ding, J. Yu, M. Wang, *Nanoscale* **2011**, 3, 1258.
- [12] A. Tampieri, G. Celotti, E. Landi, M. Sandri, N. Roveri, G. Falini, *J. Biomed. Mater. Res. - Part A* **2003**, 67, 618.
- [13] P. Ball, *Nature* **1999**, 400, 507.
- [14] D. Li, T. Cassidy, D. Bromilow, in *Ind. Des. - New Front.* (Ed: D.A. Coelho), InTech, **2011**, pp. 39–42.
- [15] F. Dehghani, N. Annabi, *Curr. Opin. Biotechnol.* **2011**, 22, 661.
- [16] R. Huang, X. Zhu, H. Tu, A. Wan, *Mater. Lett.* **2014**, 136, 126.
- [17] C. S. Tiwary, S. Kishore, S. Sarkar, D. R. Mahapatra, P. M. Ajayan, K. Chattopadhyay, *Sci. Adv.* **2015**, 1, e1400052.
- [18] M. Kaur, T. G. Yun, S. M. Han, E. L. Thomas, W. S. Kim, *Mater. Des.* **2017**, 134, 272.
- [19] S. Belhabib, S. Guessasma, *Int. J. Mech. Sci.* **2017**, 133, 728.
- [20] S. Naghieh, E. Foroozmehr, M. Badrossamay, M. Kharaziha, *Mater. Des.* **2017**, 133, 128.
- [21] S. M. Sajadi, P. S. Owuor, S. Schara, C. F. Woellner, V. Rodrigues, R. Vajtai, J. Lou, D. S. Galvão, C. S. Tiwary, P. M. Ajayan, *Adv. Mater.* **2018**, 30, 1704820.
- [22] Z. Qin, G. S. Jung, M. J. Kang, M. J. Buehler, *Sci. Adv.* **2017**, 3, e1601536.
- [23] A. L. MACKAY, H. TERRONES, *Nature* **1991**, 352, 762.
- [24] H. Terrones, M. Terrones, *New J. Phys.* **2003**, 5, 126.

- [25] G. Benedek, *Diam. Relat. Mater.* **2003**, *12*, 768.
- [26] D. C. Miller, M. Terrones, H. Terrones, *Carbon N. Y.* **2016**, *96*, 1191.
- [27] J. R. Owens, C. Daniels, A. Nicolaï, H. Terrones, V. Meunier, *Carbon N. Y.* **2016**, *96*, 998.
- [28] Z. Wang, L. Yu, W. Zhang, J. Han, Z. Zhu, G. He, Y. Chen, G. Hu, *Chem. Phys. Lett.* **2003**, *380*, 78.
- [29] M. Sharon, K. Mukhopadhyay, K. Yase, S. Iijima, Y. Ando, X. Zhao, *Carbon N. Y.* **1998**, *36*, 507.
- [30] E. F. Oliveira, P. A. S. Autreto, C. F. Woellner, D. S. Galvao, *Comput. Mater. Sci.* **2019**, *161*, 190.
- [31] F. Delodovici, N. Manini, R. S. Wittman, D. S. Choi, M. Al Fahim, L. A. Burchfield, *Carbon N. Y.* **2018**, *126*, 574.
- [32] J. F. R. V. Silveira, A. R. Muniz, *Carbon N. Y.* **2018**, *139*, 789.
- [33] E. Braun, Y. Lee, S. M. Moosavi, S. Barthel, R. Mercado, I. A. Baburin, D. M. Proserpio, B. Smit, *Proc. Natl. Acad. Sci.* **2018**, *115*, E8116.
- [34] E. F. Oliveira, P. A. da S. Autreto, C. F. Woellner, D. S. Galvao, *Carbon N. Y.* **2018**, *139*, 782.
- [35] K. Kim, T. Lee, Y. Kwon, Y. Seo, J. Song, J. K. Park, H. Lee, J. Y. Park, H. Ihee, S. J. Cho, R. Ryoo, *Nature* **2016**, *535*, 131.

- [36] G. Moon, A. Bähr, H. Tüysüz, *Chem. Mater.* **2018**, *30*, 3779.
- [37] H. Nishihara, T. Kyotani, *Chem. Commun.* **2018**, *54*, 5648.
- [38] E. F. Oliveira, L. D. Machado, R. H. Baughman, D. S. Galvao, **2019**, DOI arXiv:
- [39] W. J. Higgins, J.B.; LaPierre, R.B.; Schlenker, J.L.; Rohrman, A.C.; Wood, J.D.; Kerr, G.T.; Rohrbaugh, **1998**, pp. 446–452.
- [40] A. K. Rappe, C. J. Casewit, K. S. Colwell, W. A. Goddard, W. M. Skiff, *J. Am. Chem. Soc.* **1992**, *114*, 10024.
- [41] “Laboratory for Molecular Simulation,” can be found under <http://lms.chem.tamu.edu/cerius2.html>, **n.d.**
- [42] A. C. T. van Duin, S. Dasgupta, F. Lorant, W. A. Goddard, *J. Phys. Chem. A* **2001**, *105*, 9396.
- [43] S. Plimpton, *J. Comput. Phys.* **1995**, *117*, 1.
- [44] J. M. Romo-Herrera, M. Terrones, H. Terrones, S. Dag, V. Meunier, *Nano Lett.* **2007**, *7*, 570.
- [45] W. Humphrey, A. Dalke, K. Schulten, *J. Mol. Graph.* **1996**, *14*, 33.
- [46] O. S. Arno Zang, *Stress Field of the Earth’s Crust*, Springer Science & Business Media, **2009**.